JOURNAL OF GEOPHYSICAL RESEARCH, VOL. 107, NO. B9, 2194, doi:10.1029/2000JB000024, 2002

Estimated effects of the vertical structure of atmospheric mass on the time-variable geoid

Sean Swenson and John Wahr

Department of Physics and Cooperative Institute for Research in Environmental Sciences, University of Colorado, Boulder, Colorado, USA

Received 23 October 2000; revised 15 January 2002; accepted 20 January 2002; published 19 September 2002.

[1] The GRACE satellite mission is designed to map the Earth's gravity field at a resolution of a few hundred kilometers every 30 days beginning in 2002. At these timescales, much of the change in the gravity field may be attributed to processes involving the redistribution of water on the surface of the Earth. Contributions from continental water storage, the oceans, and the atmosphere will all be present in the time-varying gravity solutions. Isolating the hydrological and oceanographic signals will first require the removal of the atmospheric component of the gravity field estimates provided by GRACE. The vertical distribution of mass in the atmosphere is typically neglected when calculating the atmospheric gravity signal. We examine the accuracy of this approximation, as well as the accuracies of models which determine idealized atmospheric vertical structure from surface values of temperature and pressure. Using isobaric geopotential height data from a global forecast center to characterize the true atmospheric density distribution, we compute an exact atmospheric gravity signal with which to compare the gravity signal of each of these models. In addition, we examine the effects of including the aspherical component of the Earth's shape when calculating the atmospheric component of the gravity field. Because gravity estimates from GRACE will have limited spatial resolution, we average our results over regions of 200 to 500 km. At these length scales, our results show that using models based solely on surface data can introduce errors in the time variable surface mass signal inferred from GRACE as large as a few millimeters equivalent water thickness, with a global RMS of about 1 mm. *INDEX TERMS:* 1214 Geodesy and Gravity: Geopotential theory and determination; 1640 Global Change: Remote sensing; 3210 Mathematical Geophysics: Modeling; 3337 Meteorology and Atmospheric Dynamics: Numerical modeling and data assimilation; 9810 General or Miscellaneous: New fields (not classifiable under other headings); *KEYWORDS:* GRACE, satellite gravity, atmospheric pressure, time-variable gravity

Citation: Swenson, S., and J. Wahr, Estimated effects of the vertical structure of atmospheric mass on the time-variable geoid, *J. Geophys. Res.*, *107*(B9), 2194, doi:10.1029/2000JB000024, 2002.

1. Introduction

[2] The NASA and Deutsches Zentrum fur Luft und Raumfahrt (DLR) satellite gravity mission GRACE, launched in March, 2002, will map the Earth's gravity field to high accuracy and spatial resolution every 30 days. The time-variable component of these gravity solutions can be used to study surface processes that involve redistribution of water, both on the continents and in the ocean [*Wahr et al.*, 1998]. First, however, the gravitational effects of the atmosphere must be removed in order to isolate the hydrological and oceanographic signals.

[3] Typically the vertical structure of the atmosphere is ignored when computing its gravitational attraction, so that changes in atmospheric density are assumed to be confined to a negligibly thin layer at the Earth's surface. The rationale for this assumption is that the horizontal scale of atmospheric pressure variability is typically much greater than the atmospheric thickness. With this assumption, changes in atmospheric gravity can be calculated from surface pressure fields.

[4] In principle, the vertical position of an atmospheric mass anomaly does affect its gravitational signal. The effects on surface gravimeter observations were considered by, for example, *Merriam* [1992], who concluded that they were small compared with other sources of gravimeter error. The purpose of this study is to assess the importance of these effects on satellite measurements of time-variable gravity, particularly from GRACE. For example, if these effects are ignored, what is the impact on GRACE estimates of hydrological and oceanic mass variability? Is it possible to obtain improved results by employing a model which uses only surface fields to describe the vertical density profile of the atmosphere?

[5] We address these questions by using geopotential height fields to characterize the vertical distribution of atmospheric mass. We compare the gravitational solutions computed from the geopotential heights with solutions computed using models that require only surface fields to characterize the vertical structure of the atmosphere. Our

0148-0227/02/2000JB000024$09.00

results show that at scales of a few hundred kilometers and larger, these approximations introduce errors in surface mass estimates from GRACE as large as a few millimeters of equivalent water thickness, with a global RMS of about one millimeter.

2. Modeling GRACE Surface Mass Estimates

2.1. Surface Mass Component of the Geoid

[6] GRACE will use continuous measurements of the distance between two closely-spaced satellites to map out the geoid (the equipotential surface coinciding with mean sea level over the oceans) at 30-day time intervals. The geoid can be expanded in terms of spherical harmonics as

$$N(\theta,\phi) = a\sum_{l=0}^{\infty}\sum_{m=0}^{l}\tilde{P}_{lm}(\cos\theta)\{C_{lm}\cos m\phi + S_{lm}\sin m\phi\}, \quad (1)$$

where a is the Earth's mean radius, θ is colatitude, ϕ is east longitude, C_{lm} and S_{lm} are dimensionless Stokes coefficients, and $\tilde{P}_{lm}$ are normalized associated Legendre functions [see *Wahr et al.*, 1998, equation (2)]. GRACE will provide C_{lm} and S_{lm} estimates up to degree and order (l and m) of about 100, every 30 days. Spherical harmonics of degree 100 have a half-wavelength of about 200 km, while those of lower degree correspond to longer spatial scales. However, the accuracy of the GRACE estimates will degrade as l increases, so that the coefficients of the highest-resolution spherical harmonics will contain the greatest measurement errors.

[7] A hydrologist or oceanographer can use changes in C_{lm} and S_{lm} to infer changes in the distribution of water on land and in the ocean. *Wahr et al.* [1998] showed that changes in C_{lm} and S_{lm} are related to changes in the Earth's density distribution by

$$\left.\begin{matrix}\Delta C_{lm}\\ \Delta S_{lm}\end{matrix}\right\} = \frac{3}{4\pi a\rho_E}\frac{1}{(2l+1)}\int_0^{2\pi}\int_0^{\pi}\Delta I_l(\theta,\phi) \cdot \tilde{P}_{lm}(\cos\theta)\left\{\begin{matrix}\cos m\phi\\ \sin m\phi\end{matrix}\right\}\sin\theta\, d\theta\, d\phi, \quad (2)$$

where ρ_E is the average density of the Earth. ΔI_l denotes the change in the integral

$$I_l(\theta,\phi) = \int_0^{\text{top of atmos}}\left(\frac{r}{a}\right)^{l+2}\rho(r,\theta,\phi)dr, \quad (3)$$

where r is the radial coordinate, $\rho(r, \theta, \phi)$ is the density at the point (r, θ, ϕ), and the integral in equation (3) extends from the center of the Earth to the top of the atmosphere.

[8] The density field in equation (3) includes contributions from the atmosphere, from the solid Earth, and from water (including snow and ice) stored on land and in the ocean. In the solid Earth, the only nonsecular variability large enough to be detected by GRACE [*Dickey et al.*, 1997] are Earth tides, very large earthquakes, and the deformation caused by atmospheric, hydrological, and oceanic loading. The effects of Earth tides and large earthquakes can be independently modeled and removed from the data. The contributions from the load-induced deformation are related to the contributions from the load itself by Love numbers [*Wahr et al.*,1998]. Atmospheric effects will also be independently modeled and removed from the data. This study explores the importance of including the atmosphere's vertical structure during the modeling process.

[9] After removing the effects of the atmosphere and the solid Earth from the time-variable gravity data, the only remaining contributions to ΔI_l come from water stored on land and in the ocean. Changes in I_l can then be expressed as

$$\Delta I_l(\theta,\phi) = \int_{\text{thin layer}}\left(\frac{r}{a}\right)^{l+2}\Delta\rho(r,\theta,\phi)dr, \quad (4)$$

where "thin layer" refers to the region near the Earth's surface which includes all significant nonatmospheric water storage variability.

[10] This region is significantly smaller than the horizontal scale of the geoid obtained with GRACE. For example, changes in continental water storage are most likely to be important within 500 m of the Earth's surface. Changes in oceanic density can occur at all oceanic depths, so that r can, in principle, vary by as much as about 5 km. However, most oceanic mass variation is occurs at or above the thermocline, the depth of which is generally only a few hundred meters or less.

[11] Suppose we write $r = r_s + \delta r$ in the integrand of (4), where

$$r_s(\theta,\phi) = a + \xi(\theta,\phi) + h(\theta,\phi) \quad (5)$$

is the radial coordinate of the Earth's surface at (θ, ϕ), $\xi(\theta, \phi)$ is the height of the mean geoid above the mean sphere $r = a$, and $h(\theta, \phi)$ is the elevation of the Earth's surface above the mean geoid (i.e. h is the Earth's surface topography). The quantity δr, which is the height above the Earth's surface, becomes the new integration variable in (4). If we assume that $\delta r \ll a + \xi + h$, then to first order in $\delta r/(a + \xi + h)$, (4) reduces to

$$\Delta I_l \approx \left(1+\frac{\xi+h}{a}\right)^{l+2}\int_{\text{thin layer}}\left(1+\frac{(l+2)\delta r}{a+\xi+h}\right)\Delta\rho\, d\delta r. \quad (6)$$

[12] With the assumption that the thickness of the δr integration is on the order of 500 m or less for most hydrological and oceanographic processes, we find that for $l \le 100$, $(l + 2)\delta r/(a + \xi + h) \le 0.008$. Thus, to an accuracy of better than 1%, we can approximate ΔI_l as

$$\Delta I_l \approx \left(1+\frac{\xi+h}{a}\right)^{l+2}\int_{\text{thin layer}}\Delta\rho\, d\delta r = \left(1+\frac{\xi+h}{a}\right)^{l+2}\Delta\sigma, \quad (7)$$

where $\Delta\sigma(\theta, \phi) = \int \Delta\rho\, d\delta r$ can be interpreted as the change in surface mass density associated with the hydrological or oceanographic process.

[13] Suppose $\Delta\sigma$ is expanded as a sum of Legendre functions

$$\Delta\sigma(\theta,\phi) = a\rho_w\sum_{l=0}^{\infty}\sum_{m=0}^{l}\tilde{P}_{lm}(\cos\theta)\{\Delta\tilde{C}_{lm}\cos m\phi + \Delta\tilde{S}_{lm}\sin m\phi\}, \quad (8)$$

where ρ_w is the density of water and is included in (8) as a normalizing factor. Using (8) and (7) in (2), and assuming that $\xi + h = 0$ (thus ignoring the aspherical shape of the Earth's surface), *Wahr et al.* [1998] found that

$$\begin{Bmatrix} \Delta\tilde{C}_{lm} \\ \Delta\tilde{S}_{lm} \end{Bmatrix} = \frac{\rho_E}{3\rho_w} \frac{(2l+1)}{1+k_l} \begin{Bmatrix} \Delta C_{lm} \\ \Delta S_{lm} \end{Bmatrix}. \quad (9)$$

Here k_l are the Earth's load Love numbers [see, e.g., *Han and Wahr*, 1995] which account for the change in gravity induced in the solid Earth by the hydrological and oceanic load. Equation (9) can be used with ΔC_{lm} and ΔS_{lm} from GRACE to find $\Delta\tilde{C}_{lm}$ and $\Delta\tilde{S}_{lm}$, and thus learn about changes in the distribution of water on land and in the ocean.

2.2. Spatial Averaging

[14] A hydrologist or oceanographer will be interested in learning about $\Delta\sigma$. Because GRACE will not provide accurate ΔC_{lm} and ΔS_{lm} at spatial scales of less than a few hundred km, it will only be possible to learn about surface mass densities averaged over regions of a few hundred km and larger. To construct these averages we employ a method described by *Jekeli* [1981] and adopted by *Wahr et al.* [1998]. Spatial averages of surface mass, $\Delta\overline{\sigma}$, are constructed using a Gaussian averaging function, W, that depends on the angle γ between two points (θ, ϕ) and (θ', ϕ'), i.e. $\cos\gamma = \cos\theta\cos\theta' + \sin\theta\sin\theta'\cos(\phi - \phi')$,

$$\Delta\overline{\sigma}(\theta,\phi) = \int \Delta\sigma(\theta',\phi') W(\gamma) \sin\theta' d\theta' d\phi', \quad (10)$$

$$W(\gamma) = \frac{b}{2\pi} \frac{\exp[-b(1-\cos\gamma)]}{1-e^{-2b}}, \quad (11)$$

$$b = \frac{\ln(2)}{[1-\cos(r_{hw}/a)]}. \quad (12)$$

r_{hw}, the half width of the Gaussian averaging function, is the distance along the Earth's surface at which $W(\gamma) = \frac{1}{2}W(0)$. Thus r_{hw} can be loosely interpreted as the spatial scale of the averaging process.

[15] In the spherical harmonic domain, using equation (9), the expression for $\Delta\overline{\sigma}$ becomes

$$\Delta\overline{\sigma}(\theta,\phi) = \frac{2\pi a\rho_E}{3} \sum_{m=0}^{\infty}\sum_{l=m}^{\infty} \frac{2l+1}{1+k_l} W_l \tilde{P}_{lm}(\cos\theta) \cdot \{\Delta C_{lm}\cos m\phi + \Delta S_{lm}\sin m\phi\}, \quad (13)$$

where

$$W_l = \frac{1}{\sqrt{2l+1}} \int_0^{\pi} W(\gamma)\tilde{P}_{l0}(\cos\gamma)\sin\gamma\, d\gamma. \quad (14)$$

ΔC_{lm} and ΔS_{lm} provided by GRACE can be used in equation (13) to estimate $\overline{\sigma}$. Although the sum over l in equation (13) has an upper limit of $l = \infty$, GRACE will only deliver 30-day ΔC_{lm} and ΔS_{lm} for $l < 100$. Furthermore, the accuracies of ΔC_{lm} and ΔS_{lm} will decrease for large l.

[16] W_l also decrease with increasing l. For example, when $r_{hw} = 400$ km, W_{70} is less than 0.1% of W_{10}, and W_{100} is reduced by an additional three orders of magnitude [see *Wahr et al.*, 1998, Figure 3]. This decrease is more rapid for larger r_{hw}. Thus, the inclusion of W_l in equation (13) decreases the sensitivity of $\overline{\sigma}$ to the relatively inaccurate ΔC_{lm} and ΔS_{lm} at large l, and to the truncation at $l < 100$. *Wahr et al.* [1998] concluded that by choosing r_{hw} to be about 250–300 km or greater, it would be possible to estimate monthly changes in continental water storage to accuracies of better than 10 mm equivalent water thickness, and in seafloor pressure to better than 1 mbar. These accuracies improve as r_{hw} increases.

2.3. Removing the Atmospheric Component of the Geoid

[17] GRACE will not be able to separate the changing gravitational effects of the atmosphere from those of the underlying water column: both are included in the domain of integration in equation (4). If atmospheric effects are not removed using independent information, they will contaminate estimates of hydrological and oceanographic mass.

[18] Independent estimates of atmospheric variables are available from global forecast centers such as the European Center for Medium Range Weather Forecasts (ECMWF) and National Centers for Environmental Prediction (NCEP). Global, gridded fields of variables such as surface pressure, surface temperature, and geopotential height are routinely modeled and archived at 6-hour intervals. These data will be used by GRACE Project personnel to model and remove the gravitational effects of the atmosphere on the measured GRACE satellite-to-satellite distance before those measurements are used to solve for the 30-day ΔC_{lm} and ΔS_{lm} values. Errors in the atmospheric corrections, however, may leak into the 30-day hydrological and oceanographic estimates.

[19] To evaluate the atmospheric component of the radial integral (3) one may use the hydrostatic equation

$$\frac{dP}{dr} = -\rho g \quad (15)$$

to change the variable of integration from radial distance, r, to pressure, P, where g is the gravitational acceleration. Assume that the Earth is spherical, so that $g = g(r) = g_0(a/r)^2$ where g_0 is the gravitational acceleration at the Earth's mean spherical surface ($r = a$). Then

$$I_l(\theta,\phi) = -\frac{1}{g_0}\int_{P_s}^{0} \left(\frac{r}{a}\right)^{l+4} dP, \quad (16)$$

where P_s is the pressure at the Earth's surface. We use this transformation of variables because global atmospheric isobaric geopotential height fields, $\Phi(P)$, which can be used to find $r = r(P)$, are available from organizations such as the ECMWF and NCEP, whereas atmospheric density fields are not. The geopotential height, Φ, at any elevation, z, above the mean geoid is defined as

$$\Phi = \frac{1}{g_0}\int_0^z g(a+z')dz' = a\left(\frac{z}{a+z}\right). \quad (17)$$

Thus, noting that the radial coordinate is $r = a + \xi + z$ [see, e.g., *Haurwitz*, 1941]:

$$r(P) = \frac{a}{1 - \Phi(P)/a} + \xi. \tag{18}$$

Note that Φ varies between a value of $\Phi_s = ah/(a + h)$ at the Earth's surface $z = h$ to a value of $\Phi = a$ at $z = \infty$. Substituting this expression for r into (16) gives

$$I_l(\theta, \phi) = -\frac{1}{g_0} \int_{P_s}^{0} \left(\frac{a}{a - \Phi(P)} + \frac{\xi}{a} \right)^{l+4} dP. \tag{19}$$

In section 4, we will use $\Phi(P)$ from a global forecast model in equation (19) to compute gravity signals, then compare those values to gravity signals made with approximations to $\Phi(P)$ based on surface data.

3. Approximations of Radial Integrals

[20] When calculating the gravitational attraction of the atmosphere. the vertical structure of the atmosphere is generally ignored, which is equivalent to assuming the atmosphere is an infinitesimally thin layer at the Earth's surface. As an intermediate step between the thin layer atmosphere and the "true" atmosphere (as described by the geopotential height output of a global circulation model), we consider models which contain idealized vertical structure, but do not require the full three-dimensional structure from a forecast model. Specifically, we examine a two-layer atmosphere having a linear temperature gradient in the lower layer and an isothermal upper layer whose temperature is fixed at the temperature at the top of the lower layer, a one-layer atmosphere in which the temperature decays linearly from the surface, and a one-layer isothermal atmosphere.

3.1. Thin Layer Approximations to I_l

[21] To simplify the calculation of I_l, it is usual to assume that the atmosphere is confined to a thin layer at the surface of a spherical Earth. Then equation (3) becomes

$$I_l(\theta, \phi) = \int_{\text{thin layer}} \rho(r, \theta, \phi) dr = \frac{P_s(\theta, \phi)}{g_0}, \tag{20}$$

where P_s is the pressure at the surface. The surface of the Earth, of course, is not a sphere. As shown in equation (7), by including the nonspherical effects but still ignoring the thickness of the atmospheric column, we obtain

$$I_l = \left(1 + \frac{\xi + h}{a} \right)^{l+2} \int_{\text{thin layer}} \rho \, dr = \left(1 + \frac{\xi + h}{a} \right)^{l+2} \frac{P_s}{g_0}. \tag{21}$$

3.2. Two-Layer Approximation to I_l

[22] The U.S. Standard Atmosphere (1976) is an idealized, steady state, vertical atmospheric profile, chosen to represent year-round, midlatitude conditions. It predicts a vertical temperature profile which decays linearly with height from the surface to the tropopause (assumed to be at 11 km) with a lapse rate of 6.5 K/km, beyond which the temperature remains nearly constant with increasing height. For our two-layer model we assume this general form for the temperature gradient (we assume the temperature is a linear function of geopotential height, rather than of height; though the difference is slight), but we allow the lapse rate, α, and tropopause geopotential height, Φ_{trop}, to vary in time and space. To determine $P(\Phi)$ in each layer we use the ideal gas law, $\rho = P/RT$ (R is the dry air gas constant) to eliminate density from equation (15). The result is integrated over r and the definition of geopotential height (equation (17)) is used to replace r with Φ.

[23] In the lower layer, where the temperature is assumed to decrease linearly with geopotential height according to $T(\Phi) = T_s - \alpha\Phi$, we find

$$P(\Phi, \theta, \phi) = P_s(\theta, \phi) \left(1 - \frac{\alpha(\Phi - \Phi_s(\theta, \phi))}{T_s(\theta, \phi)} \right)^{\frac{g_0}{R\alpha}}, \tag{22}$$

while the pressure in the upper layer, where $T = T_{\text{trop}}$ is constant, decays exponentially:

$$P(\Phi, \theta, \phi) = e^{\frac{\Phi_{\text{trop}}(\theta,\phi) - \Phi}{\lambda(\theta,\phi)}} P_{\text{trop}}(\theta, \phi). \tag{23}$$

Here, P_{trop} is the pressure at the tropopause, and $\lambda(\theta, \phi) = RT_{\text{trop}}(\theta, \phi)/g_0$ is the atmospheric scale height. Inverting these expressions to obtain Φ as a function of P, and using the results in equation (19), we obtain

$$\begin{aligned} I_l = &\frac{P_s}{RT_s} \int_{\Phi_s}^{\Phi_{\text{trop}}} \left(\frac{a}{a - \Phi} + \frac{\xi}{a} \right)^{l+4} \left(1 - \frac{\alpha(\Phi - \Phi_s)}{T_s} \right)^{\frac{g_0}{R\alpha} - 1} d\Phi \\ &+ \frac{P_{\text{trop}}}{\lambda g_0} \int_{\Phi_{\text{trop}}}^{a} \left(\frac{a}{a - \Phi} + \frac{\xi}{a} \right)^{l+4} e^{\frac{\Phi_{\text{trop}} - \Phi}{\lambda}} d\Phi, \end{aligned} \tag{24}$$

where λ is determined by the temperature at Φ_{trop}. To implement (24), we obtain gridded values of tropopause pressure, P_{trop}. We use $P = P_{\text{trop}}$ in (22) and solve for Φ, which is then equal to the tropopause geopotential height Φ_{trop}. We use $\Phi = \Phi_{\text{trop}}$ in the temperature profile equation $T = T - \alpha\Phi$, to obtain T_{trop} and so to infer the scale height λ. We use these values, along with lapse rate estimates, and integrate (24) numerically.

[24] A difference between our model and the standard atmosphere is that the lapse rate and tropopause height are spatial and temporal constants in the standard atmosphere, while we allow both quantities to vary in time and space. Studies such as *Stone and Carlson* [1979] and *Yang and Smith* [1985] have examined the tropospheric lapse rate as a function of latitude. The similarity of the relationship between lapse rate and latitude to that between surface temperature and latitude prompted us to examine the possibility of using surface temperature to determine the tropospheric lapse rate. We modeled that temperature dependence by calculating the linear temperature gradient, α, which best fit the three-dimensional NCEP temperature fields from the surface to the tropopause at each point on the 2.5° × 2.5° grid for a given day. We used all the resulting 2.5° × 2.5° values of α for that day, and fit them simultaneously with a quadratic function of surface temperature:

$$\alpha = q_0 + q_1 T_s + q_2 T_s^2 \tag{25}$$

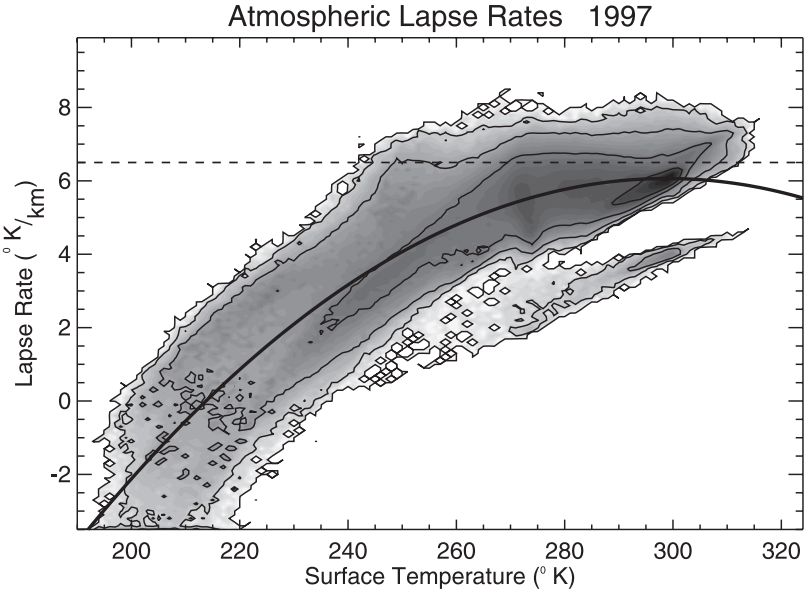

Figure 1. Contours of the logarithm of the number of grid points as a function of surface temperature and lapse rate. The solid line shows the least squares fit of lapse rate as a quadratic function of surface temperature for 1997. The dashed line shows the lapse rate used in the U.S. standard atmosphere.

where q_0, q_1, and q_2 are constants and T_s is in K, We averaged all the daily values of q_0, q_1, and q_2 during 1997, and obtained $q_0 = -6.88 \times 10^{-2}$ K/m, $q_1 = 5.01 \times 10^{-4}$ m^{-1}, and $q_2 = -8.38 \times 10^{-7}$ $(K/m)^{-1}$.

[25] Our motivation for representing α with equation (25) is evident in Figure 1, which shows values of the lapse rate as a function of surface temperature for all daily values at all grid points during 1997. In Figure 1, we have divided the x and y axes into equal-sized bins, and show contours of the logarithm of the number of grid points in each bin. Note that the lapse rate estimates clearly increase with increasing surface temperature. The solid line shows our fit to the data using equation (25). The dashed line shows the lapse rate used in the U.S. standard atmosphere. At temperatures below about 240 K there exist points where the lapse rate is best fit by $\alpha < 0$. In these cases the vertical temperature profile we are attempting to fit has a strong near-surface inversion and cannot be adequately modeled by our simple linear temperature decay model. In practice, when $\alpha < 0$, we set $\alpha = 0$.

4. Results

[26] To evaluate the effects of the approximations described above, we used 1997 NCEP Reanalysis fields provided by the NOAA-CIRES Climate Diagnostics Center, Boulder, Colorado (from their Web site at http://www.cdc.noaa.gov/). We used daily averages of geopotential heights at 17 pressure levels (from 1000 to 10 mbar), of surface-level pressure and temperature, and of tropopause pressure, all given on $2.5° \times 2.5°$ global grids.

4.1. GRACE Surface Mass Estimates

[27] After using the NCEP geopotential heights and surface pressure fields in equation (19) to calculate monthly averages of the atmospheric contributions to each C_{lm} and S_{lm}, we removed the mean, and used de-meaned C_{lm} and S_{lm} in equation (13) to compute spatially-averaged estimates of monthly surface mass variability expressed in millimeters of water (note that $\Delta\sigma/\rho_w$ is the change in surface mass density expressed as equivalent water thickness). These estimates represent the errors that a hydrologist or oceanographer would make when using GRACE to infer monthly water mass variability, if atmospheric effects were not first removed.

[28] We went through this process again using each of the approximations. The results for any one of these approximations represent the signal that would be removed from the data if that approximation were used. By taking the difference between the results obtained with these approximations, and the results obtained using the exact expression (19), we are able to assess the impact those approximations might have on hydrological and oceanographic estimates from GRACE.

[29] We chose to construct monthly averages because GRACE will provide a complete set of C_{lm} and S_{lm} every 30-days. But the 30-day GRACE estimates will not be true 30-day averages. Short-period signals will alias into each 30-day estimate in a complicated manner that depends on the GRACE orbital configuration and that cannot be predicted without detailed orbital simulations. It is thus useful to assess the adequacy of the approximations at sub-monthly periods as well. To do this, we went through this same procedure of constructing spatially-averaged surface mass estimates from the atmospheric fields, but now generating daily values during a single month (January 1997) and removing the mean for that month.

[30] The spatial averaging process is not as relevant for assessing the effects of these short-period variations as it is for the 30-day values, because a short-period signal in one region will not necessarily be aliased into a 30-day value over only that same region. Still, the spatially-averaged

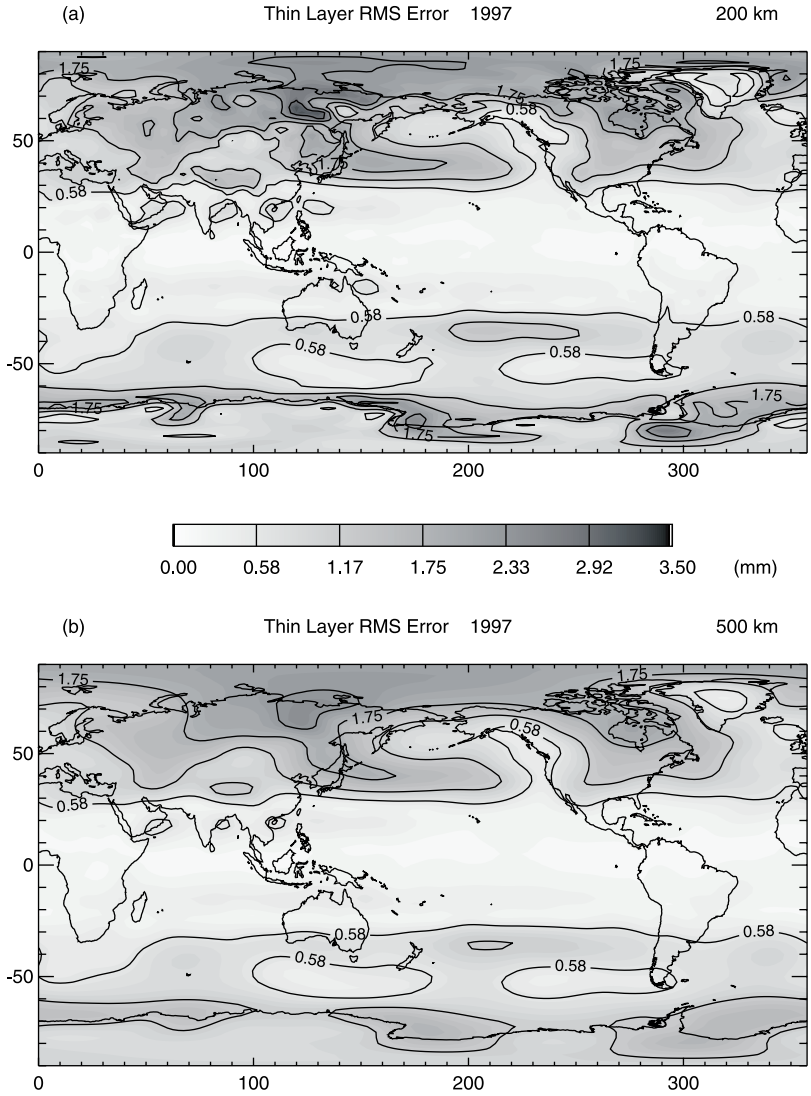

Figure 2. Estimates of surface mass error due to the use of the thin layer, spherical model when removing the atmospheric signal from GRACE measurements. (a) Contours of the RMS errors of 30-day averages for 1997, spatially averaged over 200 km regions using a Gaussian weighting function. (b) RMS errors spatially averaged over 500 km regions.

results do provide some measure of the amplitude of the short-period atmospheric error. We expect our results may over-estimate the effects, since the process of constructing 30-day GRACE values will presumably average out at least some of the short-period signal.

4.2. Thin Layer Approximation

[31] We took the difference between the 30-day spatially-averaged surface mass estimates computed using the exact expression (19), and those computed using the thin layer, spherical Earth approximation (20). These differences represent the errors in the GRACE 30-day estimates of integrated water thickness that would be caused by using (20) to remove atmospheric effects. Figure 2a shows the 1997 RMS of these errors averaged over 200 km regions (i.e., r_{hw} = 200 km in (12)). The greatest errors occur at high latitudes, with a maximum of approximately 3 mm. In the tropics the errors are <0.5 mm. The global RMS error is about 0.9 mm (Table 1). Figure 2b shows the 1997 RMS surface mass errors averaged over 500 km regions. The maximum error is reduced for this longer averaging radius to approximately 2.5 mm. The global RMS error is about 0.8 mm (Table 2).

[32] Figures 3a and 3b show RMS surface mass error estimates for the thin layer, spherical model, but this time for the January, 1997 daily values. These results represent the short-period error that could be aliased into the GRACE 30-day results (with the caveats discussed above). The results at high latitudes can be as large as 4 mm at 200 km scales, and about 2.5 mm at 500 km scales. Errors in the tropics are <0.5 mm. The global RMS error is about 1.0 mm at 200 km and 0.8 mm at 500 km (Tables 1 and 2).

[33] We made two approximations when deriving equation (20). We assumed the atmosphere was infinitesimally thin and that its lower boundary was a spherical surface. To isolate the effects of the spherical Earth assumption, we took differences between surface mass estimates obtained

Table 1. Global Spatial RMS Surface Mass Errors From 200 km Gaussian Averaging[a]

	Global	Continent	Ocean	Maximum
30-Day Errors, mm				
One-layer models				
Spherical thin layer	0.88	1.02	0.81	3.32
Aspherical thin layer	0.96	1.10	0.90	2.61
Δ thin layer	0.45	0.52	0.43	2.20
Isothermal	1.31	1.78	1.06	8.30
Lapse rate	0.82	1.11	0.66	3.36
Two-Layer Models				
Real tropopause	0.93	1.16	0.82	3.74
Parameterized tropopause	0.74	0.90	0.66	3.40
Daily Errors, mm				
One-layer models				
Spherical thin layer	1.00	1.03	0.98	3.97
Aspherical thin layer	1.12	1.08	1.14	3.73
Δ thin layer	0.91	0.86	0.93	4.67
Isothermal	1.53	2.29	1.08	9.16
Lapse rate	0.92	1.31	0.70	3.14
Two-layer models				
Real tropopause	1.26	1.64	1.07	4.40
Parameterized tropopause	0.91	1.27	0.71	4.18

[a] In mm of equivalent water thickness.

with the spherical thin layer model (20) and those computed using the nonspherical thin layer model (21). The RMS values of those differences are not shown plotted here in map form, but they have the same general spatial pattern as those shown in Figures 2 and 3: small at low latitudes and increasing at higher latitudes, particularly in the Northern Hemisphere. This spatial pattern is common to all the models we considered, and simply reflects the fact that atmospheric mass variability is larger at high latitudes. The RMS amplitudes of these differences (indicated by "Δ thin layer" in Tables 1 and 2) are about half the amplitudes shown in Figures 2 and 3.

[34] To isolate the effects of the thin layer assumption, we took differences between the surface mass estimates computed using the thin layer, nonspherical approximation (21), and those computed using the exact, nonspherical expression (19). Again, the RMS values have the same general spatial pattern as those shown in Figures 2 and 3. But their RMS amplitudes are now slightly larger than those shown in those figures (see Table 1). This implies that improving the approximation by including the Earth's nonspherical shape actually increases the RMS error.

[35] This latter result can be understood by noting that most of the RMS difference between the spherical and nonspherical thin layer models is due to the Earth's ellipticity, which affects the geoid height ξ (see equation (5)) and is the dominant aspherical component of the Earth's shape. The RMS differences due to the effects of topography are an order of magnitude smaller. The ellipticity causes the Earth's polar radius to be about 21 km smaller than its equatorial radius, with the result that most of the Earth's surface at latitudes above about 35° lies below the reference sphere ($r = a$). At those latitudes, the center of mass of the atmospheric column, which is typically several km above the Earth's surface, is closer to the Earth's mean spherical surface than it is to the real surface. Thus, the assumption of a spherical Earth in the thin layer approximation places the thin layer closer to the true center of mass of the atmospheric column, and so slightly improves the agreement with the exact results at those higher latitudes. At latitudes below about 35°, the elliptical height is positive and one might expect larger surface mass errors. However, surface pressure variation at low latitudes is minimal and so the differences between the two thin layer approximations are negligible.

4.3. Two-Layer Model

[36] Implementation of the two-layer model (24) requires values of tropopause pressure. Initially we used the NCEP 2.5° × 2.5° tropopause pressure fields. Contrary to our expectations, the errors resulting from use of this model ("shown as real troposphere" in Tables 1 and 2) were larger than the thin layer (20) errors. An examination of the NCEP tropopause data revealed areas of unexpectedly high temporal variation. In these regions, the NCEP vertical temperature profile typically consisted of a nearly linear temperature gradient in the lower atmosphere which decayed to some well defined minimum temperature above which the temperature increased linearly. This minimum was fairly constant in time. The corresponding tropopause values, however, often coincided with small kinks in the vertical temperature profile and not with the point at which the temperature gradient changed from negative to positive. The result was considerable time variation in the tropopause pressure and height.

[37] *Thuburn and Craig* [1997] calculated the tropopause height as a function of latitude using the output of a global circulation model. Again the functional form of this relationship encouraged us to attempt to regularize the tropopause data by using surface temperature to parameterize the tropopause height. We fit the tropopause pressure to a quadratic function of surface temperature just as we did the lapse rate:

$$P_{\text{trop}} = k_0 + k_1 T_s + k_2 T_s^2 \tag{26}$$

where k_0, k_1, and k_2 are constants and T_s is in K. We averaged all the daily values of k_0, k_1, and k_2 during 1997, and obtained $k_0 = -3.83 \times 10^5 Pa$, $k_1 = 3.33 \times 10^3$ Pa/K, and $k_2 = -6.75 \times 10^0$ Pa/K^2.

Table 2. Global Spatial RMS Surface Mass Errors From 500 km Gaussian Averaging[a]

	Global	Continent	Ocean	Maximum
30-Day Errors, mm				
One-layer models				
Spherical thin layer	0.82	0.98	0.74	2.53
Aspherical thin layer	0.91	1.06	0.84	2.34
Δ thin layer	0.37	0.41	0.35	1.36
Isothermal	0.89	1.29	0.66	3.45
Lapse rate	0.56	0.74	0.47	1.80
Two-layer models				
Real tropopause	0.63	0.75	0.57	1.93
Parameterized tropopause	0.50	0.58	0.46	1.81
Daily Errors, mm				
One-layer models				
Spherical thin layer	0.78	0.83	0.76	2.53
Aspherical thin layer	0.93	0.92	0.93	2.77
Δ thin layer	0.68	0.67	0.69	3.10
Isothermal	0.81	1.22	0.58	3.62
Lapse rate	0.53	0.70	0.44	1.58
Two-layer models				
Real tropopause	0.76	0.90	0.69	1.93
Parameterized tropopause	0.53	0.68	0.45	1.61

[a] In mm of equivalent water thickness.

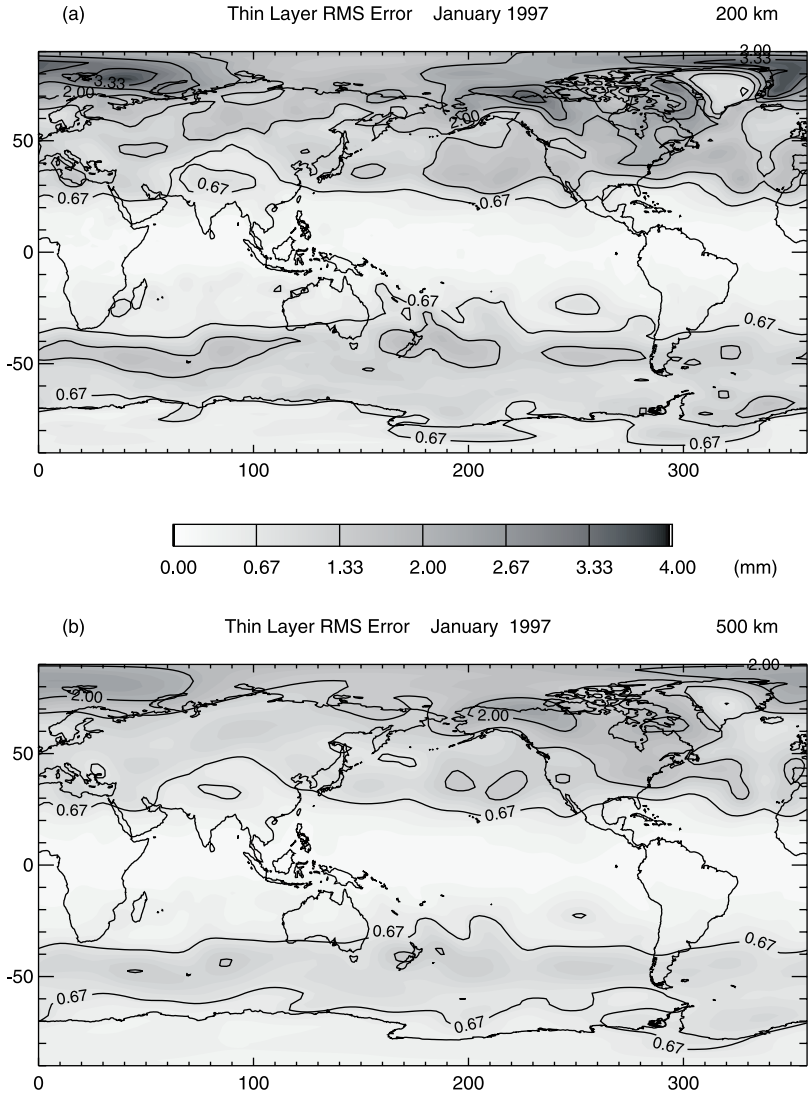

Figure 3. Similar to Figure 2 except for RMS of daily averages for January 1997.

[38] Using this parameterized tropopause in the two-layer model reduced the RMS surface mass error to 80–90% of the thin layer error. Figures 4 and 5 show the RMS surface mass errors for the two-layer atmospheric model, obtained using (25) and (26) to estimate α and P_{trop}, respectively from the NCEP surface temperature fields. Figure 4a shows the 30-day errors averaged over 200 km regions. Greatest errors occur in high latitudes, with a maximum slightly greater then 3 mm. Errors in the tropics are <0.5 mm. The global RMS error is about 0.7 mm ("parameterized tropopause" in Tables 1 and 2). Figure 4b shows the 1997 RMS surface mass error averaged over 500 km regions. Maximum error is less than 2 mm. The global RMS error is about 0.5 mm. Figure 5a shows the January 1997 RMS surface mass error averaged over 200 km regions. Errors at high latitudes approach 4 mm. Low latitude errors are <0.5 mm. The global RMS error is about 0.9 mm. Figure 5b shows the January RMS surface mass error averaged over 500 km regions. Maximum error is about 1.5 mm. The global RMS error is about 0.5 mm (Table 2). The errors here have a finer spatial scale than the errors from the thin layer approximation, due to the inclusion of surface temperature, which has greater spatial variation than does surface pressure, into the model.

4.4. One-Layer Models

[39] In addition to the two-layer model, we examined the effectiveness of using a one-layer model to approximate the vertical temperature and pressure profiles. One such model was obtained by applying a uniform temperature gradient to the entire atmospheric column. This approximation, (see "lapse rate" in Tables 1 and 2), provided results which were nearly as accurate as those of the two-layer model which utilized our parameterized values of tropopause height.

[40] In a second model, we assumed that the entire air column was isothermal (see "scale height" in Tables 1 and 2). In this case, the scale height of the atmosphere, λ, varies spatially and temporally ($\lambda(\theta, \phi) = RT_s(\theta, \phi)/g_0$ in this case). The resulting surface mass errors are greater than the surface mass errors obtained using the thin layer, spherical Earth approximation, especially at high latitudes where the isothermal errors may be twice as large as the thin layer errors.

[41] The height of the center of mass of a column of atmosphere in the isothermal model is just the scale height,

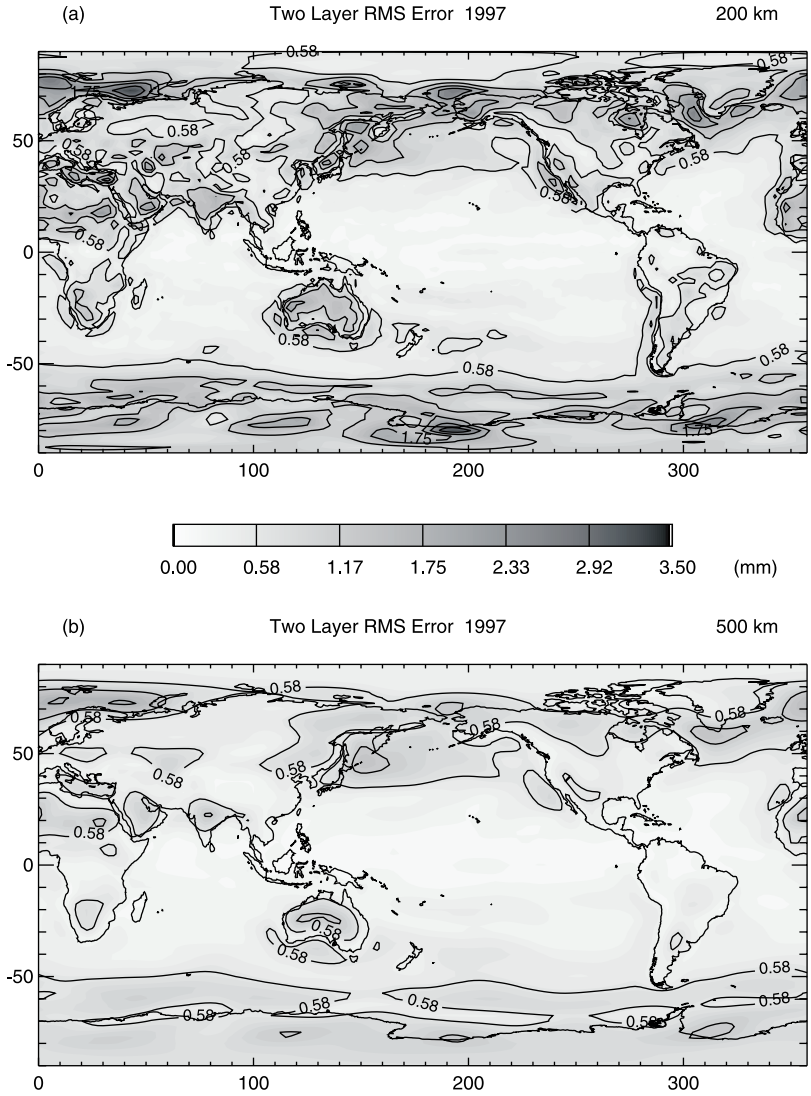

Figure 4. Estimates of surface mass error due to the use of the two-layer model when removing the atmospheric signal from GRACE measurements. (a) Contours of the RMS errors of 30-day averages for 1997, spatially averaged over a 200 km region using a Gaussian weighting function. (b) RMS errors spatially averaged over a 500 km region.

λ. Because λ is proportional to surface temperature in this case, the atmospheric gravitational potential in the isothermal model has spatial and temporal characteristics which are similar to those of the surface temperature fields. The true center of mass of a column of air is located not at the surface of the Earth but approximately one scale height above the surface; the isothermal model therefore provides a more accurate calculation of the static component of the atmosphere's gravitational potential. However, the greater errors which result from the use of the isothermal model show that this model does not improve on the thin layer model's ability to reproduce the time-variable gravitational potential.

5. Data Consistency

[42] In section 4 we described differences between exact results computed using geopotential heights, and approximate results computed assuming a thin layer atmosphere and using surface pressure fields. The differences are small for applications involving GRACE mass estimates, though for certain applications they may be large enough to justify using the exact expressions for GRACE (see section 6). But are those differences due solely to the approximations used? Or might some fraction of those differences simply reflect inconsistencies between the geopotential height and surface pressure fields output from the NCEP model?

[43] To construct the thin layer and the exact atmospheric estimates, we used three NCEP Reanalysis data sets: surface-level pressure, isobaric geopotential heights, and surface-level geopotential height (topography). To test for the effects of inconsistencies we computed these atmospheric estimates again, only using surface pressure fields derived directly from the geopotential height fields by interpolating between isobars at the surface-level geopo-

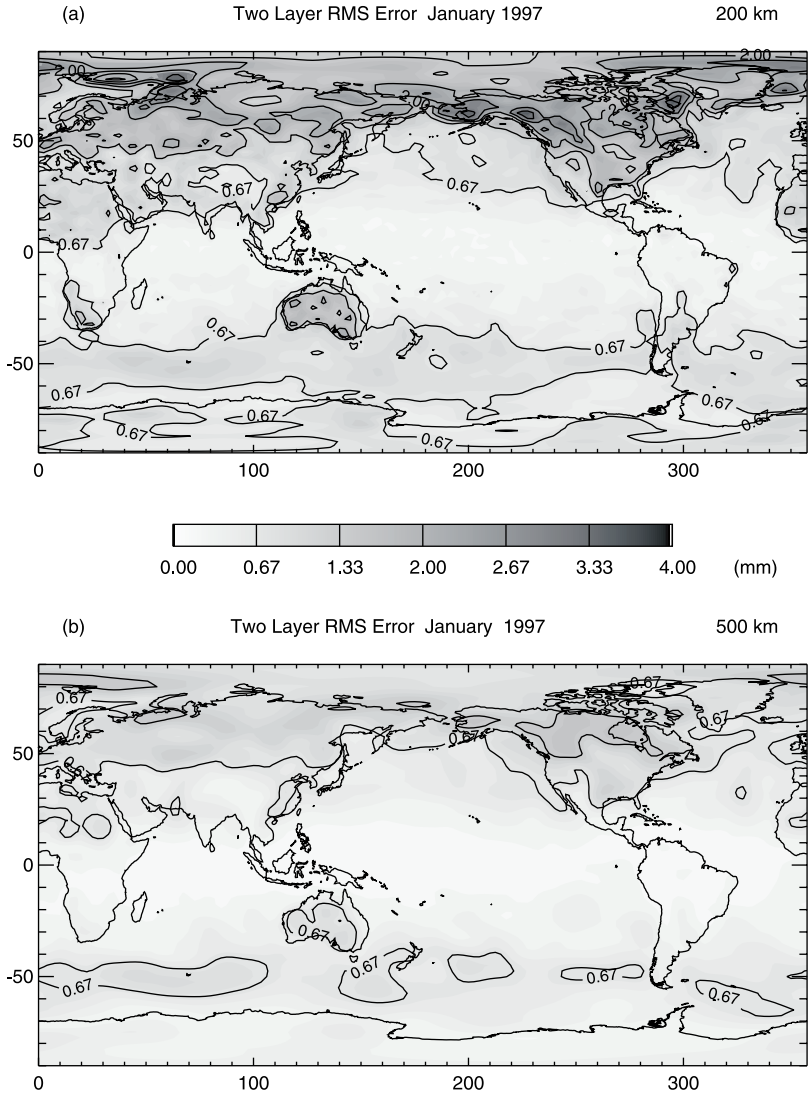

Figure 5. Similar to Figure 4 except for RMS of daily averages for January 1997.

tential height. The greatest errors approach 4 mbar and occur in regions where there exists a large gradient in elevation.

[44] We used the interpolated surface pressure fields to recompute 500 km Gaussian averages of surface mass, using both the exact expression (19) and the thin layer, spherical Earth approximation (20), and then finding the differences between these estimates. These differences should now mostly reflect the approximation error in (20). They should be relatively free of consistency problems, because the surface pressure fields in this case were obtained directly from the geopotential heights. We compared these differences with the corresponding difference we had found earlier using the original NCEP surface pressure fields (as shown in Figure 2). The RMS differences between these two difference estimates are everywhere less than 0.8 mm, with a global RMS of about 0.1 mm. We conclude, by comparing these results with those shown in Figure 3b, that whatever inconsistencies there may be between the NCEP surface pressure and geopotential height fields, they are unlikely to be inflating the error estimates shown in section 5 by more than about 10%.

6. Summary

[45] The Earth's density distribution cannot be uniquely determined solely from measurements of the Earth's external gravity field. In most cases, time-variable gravity signals detected using GRACE will originate from changes in mass at or near the Earth's surface. Even then it will not be possible to use the GRACE measurements by themselves to separate the effects of changes in water stored on land or in the ocean from the effects of mass changes in the overlying atmospheric column. Independent atmospheric information will be required to model and remove atmospheric effects from the GRACE measurements.

[46] Weather forecast centers such as NCEP and ECMWF produce isobaric geopotential height fields, which may be combined with the assumption of a hydrostatic atmosphere to yield a description of the three-dimensional atmospheric density field. However, few observations are available for

assessing the accuracy of these output geopotential fields. Additionally, the use of three-dimensional geopotential fields, rather than two dimensional surface fields, slightly increases the computational burden required to compute the atmospheric signal. It would thus be advantageous to develop a model which can reproduce the atmospheric gravity signal from surface pressure and temperature, which are better constrained by observations as well as easier to deal with computationally.

[47] Toward this end we considered approximate models of the vertical structure of the atmosphere: a model having no vertical structure (''thin layer''), an isothermal atmosphere (''scale height''), a model having a linear temperature profile (''lapse rate''), and a two-layer model combining the lapse rate and isothermal models. We found that the two-layer model based on the U.S. standard atmosphere best reproduced the results which used geopotential height fields. In each case, the global RMS difference between the models and the full calculation involving the geopotential height data is less than a millimeter. Local RMS errors may be as large as a few mm at some locations.

[48] In typical midlatitude regions such as the central United States or western Russia, seasonal hydrological signals may vary by 50–100 mm over the course of a year. In regions which experience the summer monsoon, such as India, the soil moisture signal may have a peak-to-peak amplitude of over 200 mm. Areas of central Asia such as Mongolia and northeast China, on the other hand, may have soil moisture variability less than 50 mm peak-to-peak [*Robock et al.*, 2000]. Results from a monthly, global water storage model constructed by C. Milly and A. Shmakin (personal communication, 2000) indicate that the global RMS of the continental hydrology signal is on the order of 40–50 mm for 300–500 km Gaussian averages.

[49] Because GRACE will provide monthly estimates of water storage variability that are accurate to better than 10 mm of water thickness when averaged over spatial scales larger than about 300 km [*Wahr et al.*, 1998], it is well-suited to study the hydrology signal. Although the 10 mm error estimate obtained by *Wahr et al.* [1998] was made using the spherical thin layer approximation to model errors in the GRACE atmospheric correction, our results argue that the additional error introduced by this approximation should not notably affect the solutions for continental water storage from inversion of GRACE measurements. We conclude that the use of the thin layer approximation for removing atmospheric effects will be adequate for hydrological applications.

[50] For most oceanic applications, the useful quantity inferred from GRACE measurements will be seafloor pressure, which is the total weight of the overlying oceanic and atmospheric mass. This suggests that the gravitational effects of atmospheric mass variability over the oceans should not be removed from GRACE measurements, so that those measurements can be used to provide seafloor pressure estimates. However, the relation derived by *Wahr et al.* [1998], (9), assumes that the time-variable geoid perturbations are caused by a mass anomaly having no vertical structure. Thus the results shown in Figures 2 and 3 reflect the thin layer errors over both the land and the ocean, even if the effects of atmospheric pressure over the ocean are not removed from the GRACE measurements in order to infer seafloor pressure.

[51] The time-variable gravity signal caused by mass redistribution in the ocean is smaller than that caused by changes in water stored on land [*Wahr et al.*, 1998]. Thirty-day, Gaussian averages of oceanic mass variability produced by the NCAR version of the POP ocean model [*Dukowicz and Smith*, 1994] vary by as much as 20–30 mm RMS at high-latitude locations, but are typically only on the order of 5–8 mm RMS at low latitudes. The global RMS of this variability is on the order of 10 mm for averaging radii between 300 and 500 km.

[52] In general, then, the errors caused by ignoring the atmosphere's vertical structure are about an order of magnitude smaller than the oceanic signal. This tentatively suggests that the spherical, thin layer approximation will be adequate for GRACE oceanic applications, as well. However, by using GRACE data in conjunction with data from other sources, such as ocean models and altimeters, it may be possible to explore smaller geophysical signals.

[53] For example, the total monthly seafloor pressure variability is dominated by the barotropic signal. In principle, the baroclinic component could be inferred from the GRACE measurements by subtracting results predicted by a barotropic ocean model. Thirty-day, Gaussian averages of the baroclinic component of bottom pressure from the NCAR POP ocean model are on the order of 3–5 mm RMS at low latitudes (Tierney, personal communication, 2000). The global RMS is about 7 mm for averaging radii between 300 and 500 km. In this case, the errors caused by ignoring the atmosphere's vertical structure constitute a greater fraction of the baroclinic signal.

[54] **Acknowledgments.** We wish to thank Steven Jayne, Craig Tierney, Isabella Velicogna for their contributions to this work. This work was partially supported by NASA grant NAG5-7703 and University of Texas contract UTA98-0205 both to the University of Colorado and by a CIRES Innovative Research Grant.

References

Dickey, J. O., et al., Satellite gravity and the geosphere, report, 112 pp., Natl. Res. Counc., Natl. Acad. of Sci., Washington, D.C., 1997.

Dukowicz, J. K., and R. D. Smith, Implicit free-surface method for the Bryan-Cox-Semtner ocean model, *J. Geophys. Res.*, *99*, 7991–8014, 1994.

Han, D., and J. Wahr, The viscoelastic relaxation of a realistically stratified Earth, and a further analysis of post-glacial rebound, *Geophys. J. Int.*, *120*, 287–311, 1995.

Haurwitz, B., *Dynamic Meteorology*, McGraw-Hill, New York, 1941.

Jekeli, C., Alternative methods to smooth the Earth's gravity field, *Rep. 327*, Dep. of Geod. Sci. and Surv., Ohio State Univ., Columbus, 1981.

Merriam, J. B., Atmospheric pressure and gravity, *Geophys. J. Int.*, *109*, 488–500, 1992.

Robock, A., Y. V. Konstantin, G. Srinivasan, J. K. Entin, S. E. Hollinger, N. A. Speranskaya, S. Liu, and A. Namkhai, The global soil moisture data bank, *Bull. Am. Meteorol. Soc.*, *81*, 1281–1299, 2000.

Stone, P. H., and J. H. Carlson, Atmospheric lapse rate regimes and their parameterization, *J. Atmos. Sci.*, *36*, 415–423, 1979.

Thuburn, J., and G. C. Craig, GCM tests of theories for the height of the tropopause, *J. Atmos. Sci.*, *54*, 869–882, 1997.

Wahr, J. M., The effects of the atmosphere and oceans on the Earth's wobble, I, Theory, *Geophys. J. R. Astron. Soc.*, *70*, 349–372, 1982.

Wahr, J., M. Molenaar, and F. Bryan, Time variability of the Earth's gravity field: Hydrological and oceanic effects and their possible detection using GRACE, *J. Geophys. Res.*, *103*, 30,205–30,229, 1998.

Yang, S., and G. L. Smith, Further study on atmospheric lapse rate regimes, *J. Atmos. Sci.*, *42*, 961–965, 1985.

S. Swenson and J. Wahr, Department of Physics, University of Colorado, Campus Box 390, Boulder, CO 80309-0390, USA. (swensosc@colorado.edu; wahr@lemond.Colorado.edu)